Subcortical activity during the process of coma recovery can be partitioned into distinct network states associated with arousal

Justin D. Yi, Sangwoo Han, Guilian Tian, Francisco Aguirre, Alexander Liu, Afsheen Bazrafkan, Matine Azadian, Monica Desai, Tameena Wais, Ashar Ahmed Khan, Yusuf Suri, Niki Maki, Masih Rafi, Oswald Stewart, Yama Akbari

Abstract

Background: Cardiac arrest (CA) causes debilitating neurological injury, including coma brought about by global cerebral ischemia. Subcortical brain activity, particularly in the brainstem arousal centers and their ascending projections, is key to understanding coma pathophysiology. However, a unified picture of how subcortical brain structures, like the locus coeruleus (LC), hippocampus, and thalamus, facilitate the transition out of post-CA coma is as of yet unclear.

Methods: Rats were exposed to 8 minutes of CA induced by asphyxiation and subsequently resuscitated. Then at 2, 4, 24, and 72 hours, the neurological outcome of the rats was assessed. Rats were then sacrificed for quantitative c-Fos immunofluorescence in major brainstem, hypothalamus, basal ganglia, and limbic structures. Non-negative matrix factorization (NMF) was used for dimensionality reduction. A stochastic differential equation (SDE) model was fitted to the trajectory of the latent NMF projection. Multivariate Guassians were used to calculate the covariance in the latent space as a function of time and then projected back into the full-dimensional space to estimate functional connectivity (FC).

Results: c-Fos expression peaked 2-4 hours after CA, and decayed close to baseline within 72 hours in all brain regions except the LC and hippocampal cornu Ammonis 1 (CA1). Unexpectedly, regions not previously thought to be critical for arousal, such as the hippocampal, tectal, and limbic nuclei, also exhibited c-Fos expression during coma. NMF revealed two distinct dynamic network states. The network state containing selectively elevated LC and CA1 c-Fos activity predominated 24-72 hours after coma was associated with better neurological function. An SDE model in the NMF latent-space successfully captured the dynamics of the c-Fos activity along a 2D “manifold.”

Conclusions: We demonstrate functional network activity during anoxic coma can be partitioned into at least two states, and that LC and hippocampus activity are associated with greater arousal. Subcortical c-Fos activity lives on a manifold with stereotyped dynamics in time following CA. We demonstrated that SDE simulations in the latent space were able to interpolate between sparse “snapshots” of activity to yield robust estimates of FC in the full-dimensional space even with low sample sizes. These findings may inform future methods to get a dynamic picture of coma recovery in human patients by overcoming the fact that patients can only tolerate limited time in functional brain scanners.

Graphical Abstract

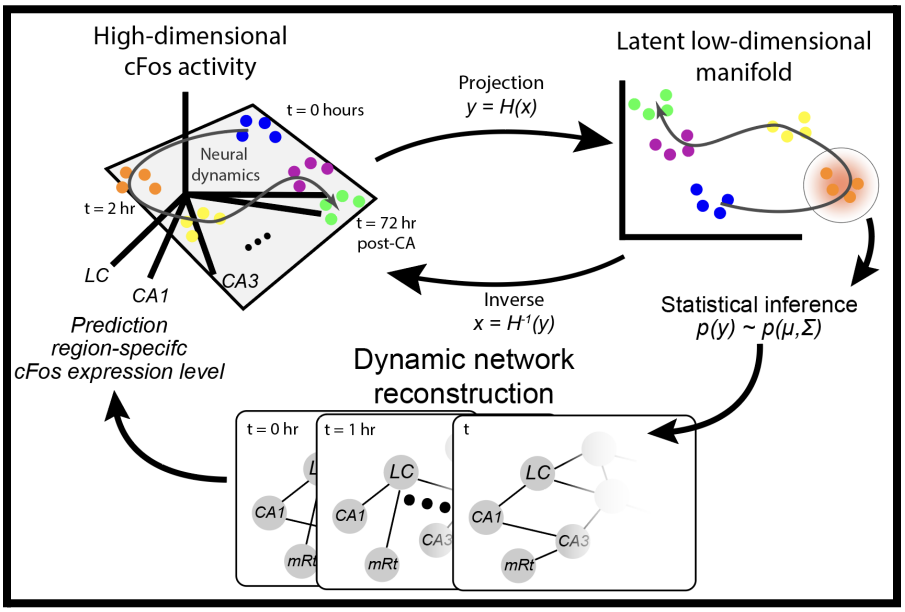

Introduction

Coma is a state of deep unconsciousness in which an individual lacks arousal. In this state, there is absence of wakefulness or ability to consciously feel, hear, move, or speak[1]. Clinical coma is defined by a Glasgow coma scale below 9 where patients lack a sleep-wake cycle, voluntary eye-opening, and the ability to respond to tactile or verbal stimuli[2]. Cardiac arrest (CA) causes loss of spontaneous circulation and global ischemia, which can lead to coma. In the United States, CA is the third most common cause of death with reportedly over half a million annual cases[3]. More than 50% of CAs occur outside of hospitals and are met with a < 6% chance of survival; this rises to just below 25% in hospital settings, as response time to treatment is decreased[4]. Current standard of care after CA includes targeted core body temperature and supportive therapy;[5] however, many survivors of CA emerge in a comatose state, and there is no current standard treatment for neurological recovery[6]. Although our previous work has shown that coma recovery is dependent on the orexin pathway[7], mechanisms of coma still remain largely unknown[7].

The reticular activating system (RAS) contains the most well-known brain regions for regulating wakefulness[8,9] as lesions in RAS have been shown to cause decreased wakefulness[10]. However, regions outside of RAS have also been implicated for arousal. A 1946 study was the first to question previous work, which had previously suggested the hypothalamus (HTh) did not play a role in arousal. This study showed lesions to the posterior HTh caused excessive sleepiness and proposed that the HTh is regularly inhibited by sleep-promoting preoptic neurons[11], while more recent reviews show that the hypothalamus is involved with regulation of the sleep-wake cycle[12]. A recent review concurs with this idea and identified specific regions of the HTh, many of which are known RAS regions[13]. Various other regions, such as the inferior colliculus (IC), have also been shown to play a role in wakefulness[14].

Given that there is still a lack of knowledge surrounding mechanisms of coma and arousal, it may be beneficial to identify additional regions pertaining to arousal, which may serve as new targets for coma therapies. In this study, we identified such brain regions using the c-Fos protein, which is an immediate early gene expressed by active neurons[15–17]. It has been shown to be expressed following cerebral ischemia, and its expression can be induced by stimuli[15]. In CA, cerebral ischemia leads to a coma, but as the brain begins to re-awaken, cFos is expressed in regions of arousal and can be identified by the cFos stain[15,17,18]. Studies investigating activated brain regions during recovery from cerebral ischemia and/or coma have been previously done, however, these studies either lacked sufficient negative controls, covered only a few brain regions, or tested only a short time post ischemia[16,17,19–22]. In this study, we employed 3 different negative controls, examined the whole brain, and tested up to 72 h post ischemia to provide a more comprehensive mapping of the specific brain regions activated during coma or early coma recovery induced by global cerebral ischemia from CA by analyzing c-Fos expression.

Results

Early coma recovery is characterized by severe neurological deficit and diffuse subcortical activation

Coma-induction was achieved through 8-minutes of asphyxial cardiac arrest (CA), as previously described by our lab[23–30]. After successful cardiopulmonary resuscitation (CPR), rats were allowed to recover gradually. Typically, unconsciousness ensued for 1–2 hours following cardiac arrest. In the

period between 2–4 hours, rats were generally impaired with Neurological Deficit scores (NDS) of 22 ± 3 [n = 6] and 27 ± 2 [n = 7] (mean ± standard error), respectively, out of a control score of 80 ["perfect" score, see Methods, n = 5]. These impairments could not be explained by anesthesia or possible post-surgical complications alone, since rats ("sham-AR") with surgery, anesthesia, chest compressions, but no asphyxia had NDS of 74 ± 3 [n = 7] after 2 hours.

Interestingly, we found that all subcortical brain regions sampled had elevated c-Fos expression in this 2–4 hour period. Expectedly, brain regions in the reticular activating system (RAS), in which ascending activity is critical for promoting arousal [31,32], was significantly elevated compared to control and sham animals (**Fig. 1**). Surprisingly, structures outside the RAS, including the hippocampus (CA1 & 3, dentate gyrus [DG]), central amygdala (CeA), caudoputamen (CPu), ventromedial hypothalamus (VMH) and superior & inferior colliculi (S/IC) all also had significantly elevated c-Fos expression at 2–4 hours (**Fig. 2**).

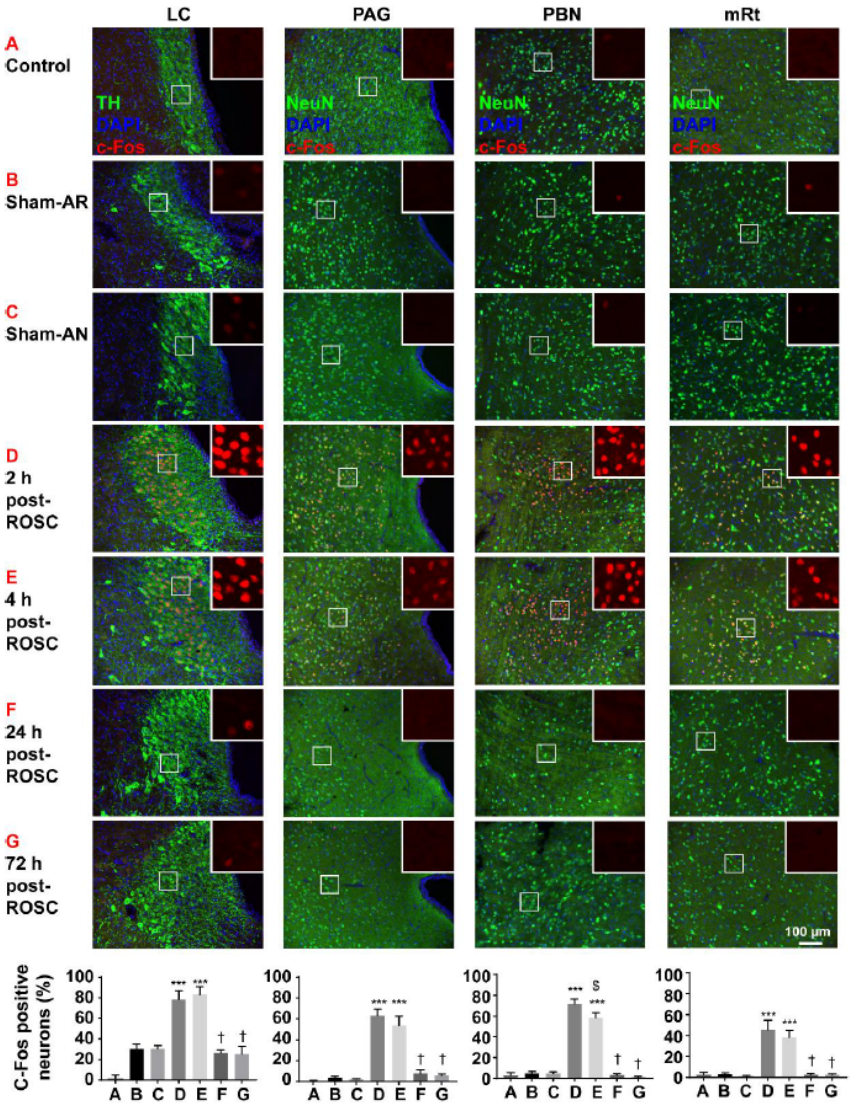

Figure 1. Activated RAS regions during coma (2 and 4 h post-ROSC). Brain sections containing LC, PAG, PBN, and mRt were co-labeled with antibody against c-Fos (red) and antibody for neuronal marker (tyrosine hydroxylase, TH, green (LC only); NeuN, green, neuronal marker for PAG, PBN, and mRt). DAPI (blue) was used as a nucleus indicator. *** p<0.001, vs control and vs sham-AR and vs sham-AN; Tukey test. † p<0.001, vs 2 h and vs 4 h; Tukey test. $ p<0.05, vs 2 h; Tukey test.

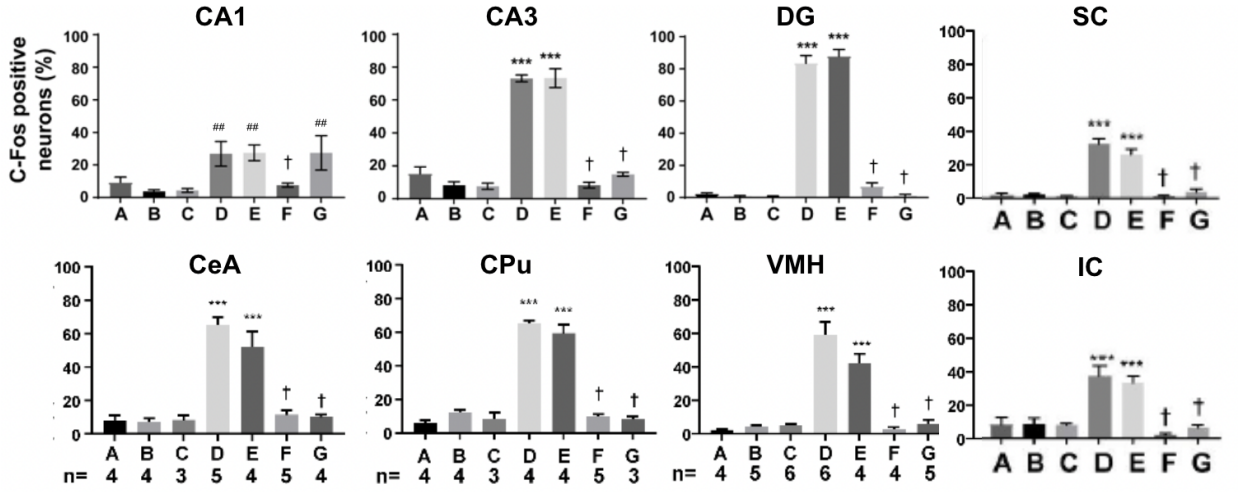

Figure 2. Brain regions outside the RAS are also diffusely activated 2–4 hours post-CA. Brain sections containing the hippocampus (CA1, CA3, DG), CeA, CPu, VMH, SC, and IC were used to quantify c-Fos immunofluorescence. *** p<0.001, ## p<0.01, vs control and vs sham-AR and vs sham-AN; Tukey test. † p<0.001, vs 2 h and vs 4 h; Tukey test.

Two "subnetworks" trade-off activity as recovery progresses

Given the relatively large number of brain regions sampled at regular intervals, the above results are combinatorially complex and hard to place into a coherent framework (**Fig. 3A**). Therefore, we used non-negative matrix factorization (NMF) as a dimensionality reduction tool to analyze temporal patterns in the network. NMF yielded two features, which correspond to a 2-D plane where rats were cleanly clustered according to their post-CA time (**Fig. 3B**). The first NMF feature corresponded to near pan-activation, and dominated at 2–4 hours, consistent with the pattern of activation seen in the raw c-Fos levels (**Fig 3C**). The second NMF feature had activity dominating in the LC and CA1, whereas other brain regions were suppressed. This second feature seemed to be associated with the later time points (24–72 hours) when there was more behavioral arousal as measured by NDS (24 hours: 55 ± 4 [n = 8], 72 hours: 72 ± 5 [n = 6]).

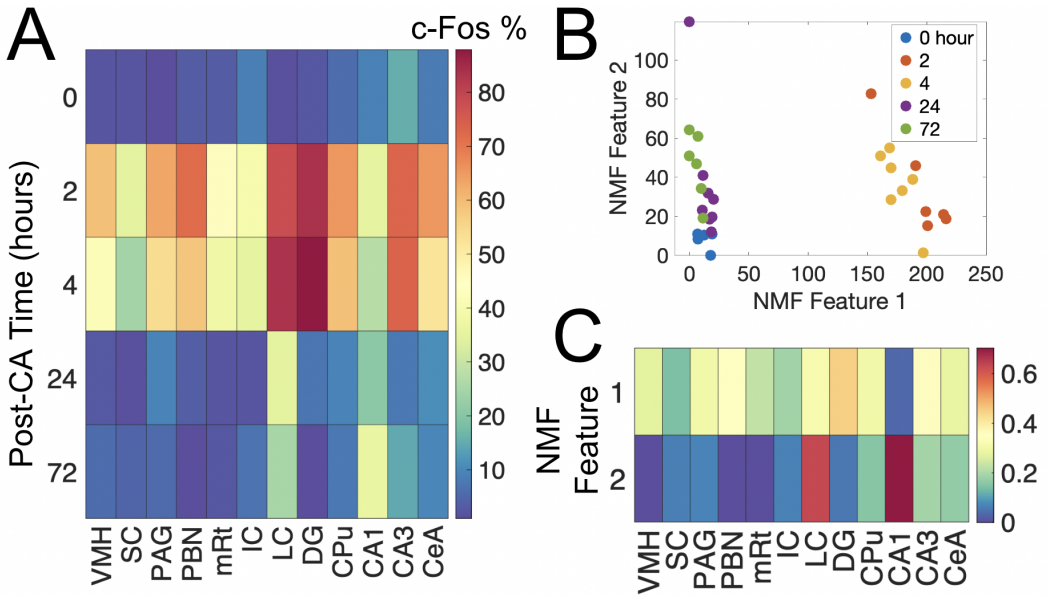

Figure 3. Dimensionality reduction of c-Fos levels reveals clusters that correspond to post-CA time. (A) The mean levels of c-Fos positivity in each brain region, stratified by post-CA time. 0 hours corresponds to control rats only. (B) A scatter plot rat's c-Fos level projected into a 2-D latent plane by NMF, colored by post-CA time, and (C) the corresponding loading for each axis.

We wanted to better understand the temporal progression of c-Fos activity in the network as a function of time. To accomplish this, we sought to build a model that could interpolate between our discrete measurements. Firstly, as detailed in the Material and Methods, we approximated each cluster in **Fig. 3B** as a multivariate Gaussian distribution with diagonal covariance. This gave us estimates of the mean and variances as a function of time. Then, we used a stochastic differential equation to encode how the probability distribution evolved through the latent space. Parameters were estimated using simulated annealing, yielding the continuous distribution seen in **Figure 4.**

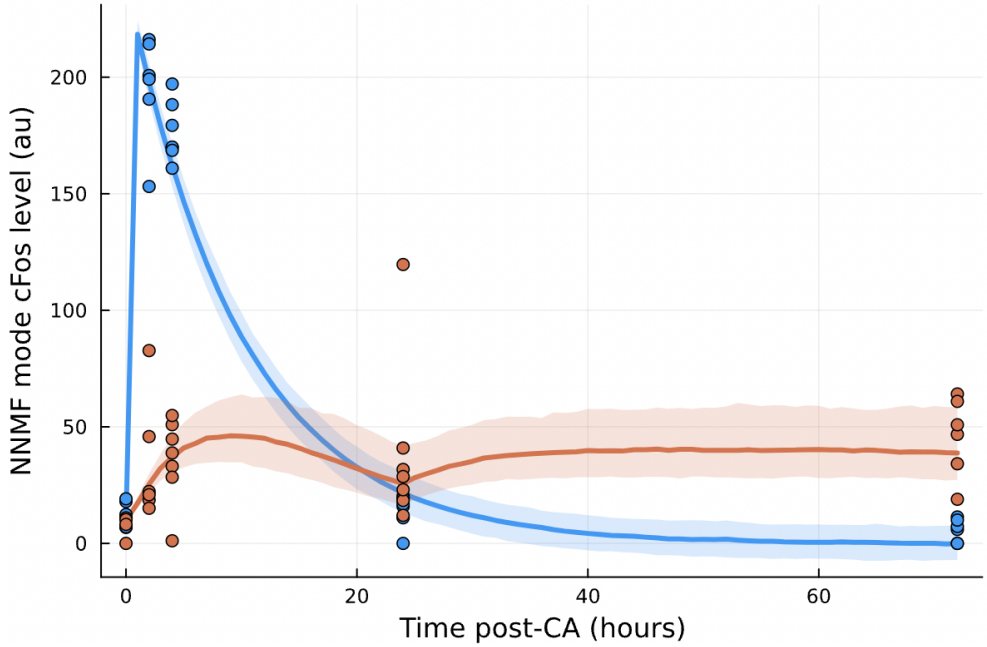

Figure 4. SDE model of the latent NMF features as a function of time. The dynamics of the first (blue) and second (orange) NMF features found in **Fig. 3B-C**. Dots correspond to c-Fos measurements projecting into the 2-D plane, whereas the solid lines and shaded regions indicate the means and 95% quantiles of the simulated SDE model.

Prominent correlated activity between the LC and higher structures emerges after 24 hours

The NMF coupled with the continuous SDE dynamics provide us a natural framework to probe the dynamics of the full c-Fos network simply by projecting the latent dynamics up into the full-dimensional sample space. Concretely, the estimates of the means and variances as in **Figures 3** and **4** can be projected up by inverting the NMF, as detailed in the Materials and Methods. At each “slice” of time in the SDE simulation, the results of projection yield a 12-dimensional Gaussian distribution. The resulting covariance matrices provide an estimate of functional connectivity (FC) between brain regions. Interestingly, for control animals, c-Fos levels and estimated FC were both low (**Fig. 5**). After c-Fos levels peaked at 2–4 hours, robust covariances between LC, CA1, CA3, and CeA emerged at 24–72 hours (**Fig. 5**), in spite of low absolute levels of c-Fos.

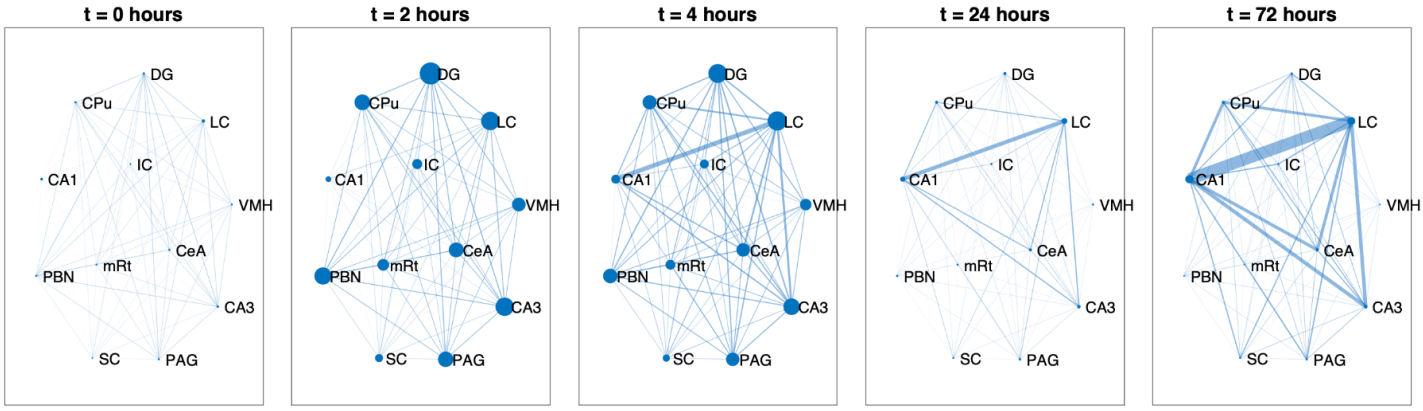

Figure 5. Functional connectivity estimates from multivariate Guassian covariances. Each panel shows a "snapshot" of the covariance matrix, where the vertex size is proportional to the mean c-Fos level at that time, and the edge width is proportional to the covariance between the nodes, estimated by inverting the NMF.

Discussion

Materials and Methods

Cardiac Arrest Experiments

Animals

A total of 45 male Wistar rats (weighing 300-400g) were obtained from Charles River Laboratories for this study. Rats were given food *ad libitum*, although food intake was restricted to 25% of normal nightly caloric intake during the 14 hours preceding cardiac arrest procedure to control for glucose levels.

Cardiac Arrest

Rats were anesthetized for 15-20 minutes prior to intubation. The first 4 minutes with 5% isoflurane carried by 100% oxygen at 4 liters per minute, and for the remaining time, reduced to 3% isoflurane and 1 liter per minute. Respiratory rate along with a qualitative evaluation of pulmonary function were used to monitor depth of anesthetization. Rats were then immediately intubated and connected to a Kent Scientific TOPO small animal ventilator with pressure set between 12-14 cmH2O depending on pulmonary function and rat weight. Respiratory rate was set at 70 breaths per minute, and flow rate at 2 liters per minute. Rats were under anesthesia using the ventilator with 2% isoflurane for the duration of the surgery carried by 50% oxygen and 50% nitrogen. Body temperature was regulated to maintain 37.0-37.5 °C.

A 3 cm diagonal incision made to the left femoral area of the rats to access the femoral artery and vein, which were catheterized using PE-20 tubing. The catheter was connected to a blood pressure transducer (CWE Inc.) attached to a pressurized, heparinized 0.9% sterile saline bag (2000 units/ml conc.), while the vein catheter was connected to a three-way stopcock attached to two syringes to allow delivery of all drugs needed during the cardiac arrest procedure. Once catheterized, animals had blood drawn for an arterial blood gas test using a Vetscan i-STAT blood gas analyzer (Abaxis). Using the measures of pH, pCO_2, pO_2, and HCO_3, the ventilator was adjusted to normalize blood chemistry for the start of the cardiac arrest procedure.

The cardiac arrest procedure began with minimizing isoflurane from 1% in order to increase EEG activity. At experimental time zero, nitrogen was turned off and oxygen was increased to 100%. After

two minutes, with the EEG nearly fully active, isoflurane was turned off, the inlet of the ventilator was disconnected in order to deliver room air to the animals, and 1 ml of vecuronium was delivered intravenously along with a 1 ml heparinized saline flush. The EEG was allowed to become fully active and free from any effects of isoflurane to accurately represent normal EEG activity during the procedure. Vecuronium was used as a neuromuscular blocker to prevent animal movement while isoflurane was off, and the EEG was active. After 3 more minutes, when EEG was fully active, the ventilator is powered off, and the ventilator tubing to the animals were clamped to simulate asphyxia. After 7 minutes of asphyxia, the ventilator was turned back on, and after 8 total minutes of asphyxia, the rats were resuscitated using CPR, 0.4 ml epinephrine, and 0.5 ml bicarbonate.

After return of spontaneous circulation (ROSC), rats were decannulated and extubated during recovery. Rats were monitored, given fluids and soaked pellets during the subsequent days to maintain hydration if immobile. To empirically monitor the recovery process, rats had neurological deficit scale (NDS) tests performed at the 2, 4, 24, and 72 hour marks (**Fig. 6**, CA). Experiments were concluded after the NDS test was done at the rats' designated time points, and rats were perfused according to the procedures below with n=6 for 2 hr, n=7 for 4 hr, n=8 for 24 hr, n=6 for 72 hr time points.

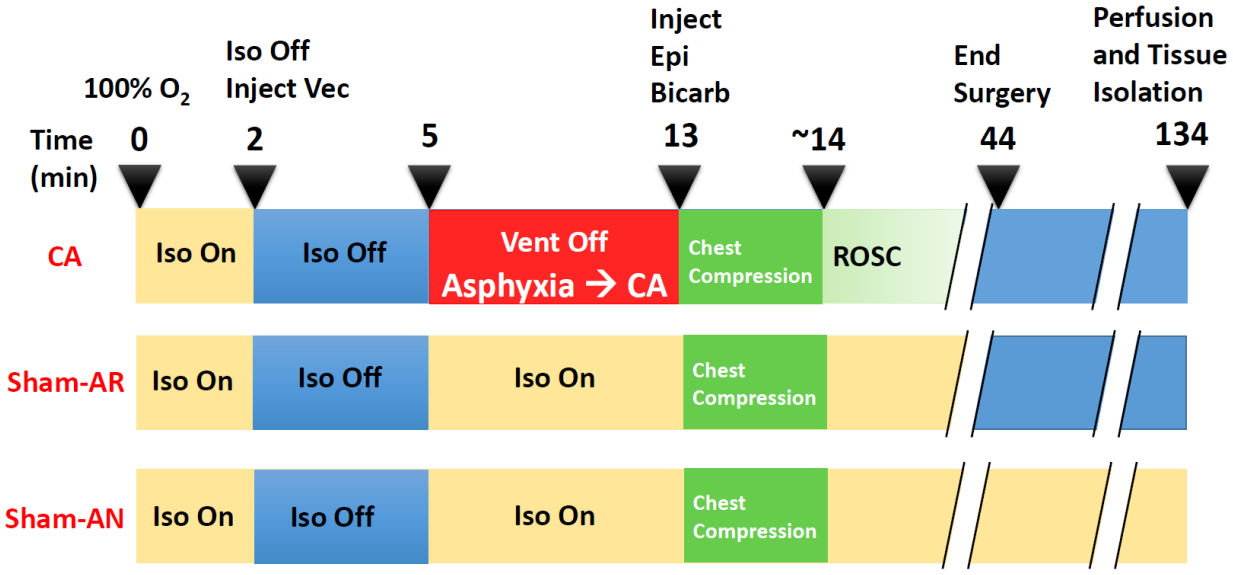

Figure 6. Experimental design. Rats were separated into 3 groups: asphyxial coma (CA), sham arousal (sham-AR), and anesthesia coma (sham-AN). All rats were under anesthesia using isoflurane (2 min) and underwent the same surgery including cannulation and intubation. Isoflurane was turned off at t=2 min to begin wash out and vecuronium (Vec) was injected to induce muscle paralysis (until t=5 min). For the asphyxial coma group (CA), ventilation was turned off to induce asphyxial CA for 8 min (t=5 – 13 min). Chest compressions were then applied and injections were given for about 1 min until ROSC. Rats were decannulated about 30 min post-ROSC (t=44 min) and perfused at various times (i.e, 2, 4, 24, and 72 h) post-ROSC. Both shams differed from CA in that at t=5 min isoflurane was turned back on and ventilation was not turned off. Both groups still received chest compressions and injections at t=13 min and were perfused at 2 h post-ROSC. Sham groups differed in that sham-AR was removed from isoflurane after decannulation about 30 min post-ROSC. Sham-AN received isoflurane until the point of perfusion, approximately 2 h post-ROSC. The sham groups allowed us to analyze brains that re-gained arousal (sham-AR) compared to those that did not regain arousal (i.e., unconscious state, sham-AN).

Sham-AR/AN and control experiments

All procedures remained the same for the sham experiments except for the induction of cardiac arrest. Instead of asphyxia, isoflurane was turned back on. During this time, all other procedures remained the same, including a period of chest compressions. Sham-AR animals (n = 7) had isoflurane turned off at the conclusion of the surgery, while Sham-AN (n = 7) animals received

isoflurane until perfusion. Both sham groups were perfused at the 2-hr post-ROSC time point (**Fig. 6**, Sham-AR and Sham-AN).

Control animals (n = 5) had no experimental procedures performed on them, except caloric restriction, before perfusion. In addition to caloric restriction before the experimental day, they also had total caloric restriction 6 hours (8 am to 2 pm) before perfusion.

Neurological evaluation

Neurological deficit score (NDS) (Table 1) was used to quantify arousal and neurological recovery. This evaluation includes components such as arousal, functions of brainstem, behavior, motor, and senses. NDS was measured right before perfusion (at 2 h post-ROSC for sham-AR; at 2, 4, 24, and 72 h post-ROSC for CA). Sham-AN scores were not measured because these rats were under anesthesia (ventilation with isoflurane)-induced unconsciousness until perfusion. Measurements for all groups were completed by at least two well-trained personnel.

Assesment	Component	Subscore	Total
A. Seizures	Seizures	None (10) / Focal (5) / Generalized (0)	_ / 10
B. Arousal	Consciousness	Normal (10) / Lethargic (5) / Comatose (0)	_ / 19
	Respiration	Normal (6) / Abnormal (3) / Absent (0)	
	Eyes	Open Independently (3) / Open to pain (1) / Absent (0)	
C. Branstem	Startle Reflex	Present (3) / Absent (0)	_ / 21
	Vision Reflex	Present (3) / Absent (0)	
	Pupillary Reflex	Present (3) / Absent (0)	
	Corneal Reflex	Present (3) / Absent (0)	
	Olfaction	Present (3) / Absent (0)	
	Whisker Stimulation	Present (3) / Absent (0)	
	Swallowing	Present (3) / Absent (0)	
D. Behavioral	Righting Reflex	Normal (3) / Abnormal (1) / Absent (0)	_ / 12
	Negative Reflex	Normal (3) / Abnormal (1) / Absent (0)	
	Spatial Awareness	Normal (3) / Abnormal (1) / Absent (0)	
	Turning Alley	Normal (3) / Abnormal (1) / Absent (0)	
E. Motor	Limbs	Normal (3) / Weak (1) / No Movement (0)	_ / 6
F. Sensory	Pain Response	Brisk (3) / Weak (1) / No Movement (0)	_ / 6
G. Motor Beh	Gait	Normal (3) / Abnormal (1) / Absent (0)	_ / 6
	Balance on Beam	Normal (3) / Abnormal (1) / Absent (0)	
		Grand Total	_ / 80

Table 1: NDS Evaluation. Seven categories are assessed with a total maximum score of 80. In general, if the NDS is below 45, the animal is considered comatose.

Histology and Immunofluorescence

Brain tissue collection

Euthanization was done via intraperitoneal injection of Euthasol (1 mL/kg; NDC 66794-013-25; Pramal/Healthcare, Mumbai, India). After 3 min, absence of withdrawal in response to paw pinch was tested and animals were transcardially perfused using 1x phosphate-buffered saline (PBS: 137 mM NaCl, 2.7 mM KCl, 10 mM Na_2HPO_4, 1.8 mM KH_2PO_4; pH 7.4) for 4 min. Brains were dissected immediately after perfusion. Right hemispheres were flash-frozen in dry ice, while eft hemispheres were fixed in 4% paraformaldehyde for 24 h at 4°C. Fixed brains were transferred to 30% sucrose for 3 days and were then frozen in optimal cutting temperature (OCT) medium and kept at -80°C until sectioning.

Section Collection

Brains were coronally sectioned at 30 µm using a cryostat (Microtome HM 505N) and stored serially in a 96-well plate in a 1x PBS · NaN3 solution at 4°C. 3 sections, spaced 120 µm apart, were chosen per rat. From the prefrontal cortex to the spinal cord, every 12th section was picked. A total of about

81 sections covering the whole brain were examined for each timepoint. Based on “The Rat Brain in Stereotaxic Coordinates, 6th Edition” by Paxinos and Watson, sections containing the following brain regions were chosen to be analyzed: locus coeruleus (LC; bregma -9.86 mm); parabrachial nucleus (PBN) and inferior colliculus (IC) (bregma -8.76 mm); superior colliculus (SC), periaqueductal gray (PAG), and mesencephalic reticular thalamus (mRt) (bregma -6.96 mm); CA1, CA3, dentate gyrus (DG), central amygdala (CeA), caudate putamen (CPu), and ventromedial hypothalamus (VMH).

Immunofluorescence

Sections were blocked using 3% donkey serum (DS) in 0.3% PBST (0.3% Triton X-100 in 1x PBS) for 1 h at room temperature (RT), then incubated overnight with primary antibodies in 0.3% PBST + 1% DS at 4 °C. Sections were washed 3 times in a 0.1% PBST (0.1% Triton X-100 in 1X PBS) bath then incubated with secondary antibodies and DAPI (1mg/mL in 1x PBS, 62248, Thermo Fisher Scientific, Waltham, MA) in 0.3% PBST + 1% DS for 1 h at RT. Sections were then washed 3 times in a 0.1% PBST bath.

Primary antibodies: LC: mouse anti-c-Fos antibody (Sc-271243, Santa Cruz Biotechnology, Santa Cruz, CA) and rabbit anti-tyrosine hydroxylase antibody (ab112, Abcam, Cambridge, MA);, PBN: rabbit anti-c-Fos antibody (ABE457, MilliporeSigma, Burlington, MA), and mouse anti-NeuN antibody (MAB377, MilliporeSigma, Burlington, MA),; PVN: mouse anti-c-Fos antibody (Sc-271243, Santa Cruz Biotechnology, Santa Cruz, CA), and rabbit anti-oxytocin antibody (AB911, MilliporeSigma, Burlington, MA); All other regions: mouse anti-c-Fos antibody (Sc-271243, Santa Cruz Biotechnology, Santa Cruz, CA) a and rabbit anti-NeuN antibody (ab177487, Abcam, Cambridge, MA).

Secondary antibodies: Alexa Fluor 488 donkey anti-rabbit immunoglobulin G (IgG; A21206, Life Technologies, Carlsbad, CA) and Cy3 donkey anti-mouse IgG (715-165-150, Jackson ImmunoResearch, West Grove, PA).

Once stained, sections were mounted on Superfrost Plus Micro Slides (48311-703, VWR, Radnor, PA) and left to dry. To rehydrate for coverslipping, slides were placed in a 1x PBS bath for 10 min. Coverslips (48393-251, VWR, Radnor, PA) were placed along with Vectashield mounting medium (H-1000; Vector Laboratories, Burlingame, CA) for storage.

Cell Counting

LC and PBN regions were imaged by a Nikon Eclipse Ti-E microscope while other regions were stitched using images taken from Keyence FL microscope 2.0. Fluorescence blurring was reduced using the same haze reduction function for all images. Brain regions of interest were divided into numbered dissectors; half of these were selected for cell counting by a random number generator. Within each chosen dissector, total neurons (NeuN or TH), c-Fos positive neurons were counted using the ImageJ “Cell Counter” plugin. To avoid over-counting, positive cells on the left or bottom dissector were omitted from counting. Results are presented as a percent of: # c-Fos positive / # total neurons.

Statistical Analyses

Software

All analyses were performed in MATLAB (R2022b, MathWorks, Natick, MI) and Julia (Version 1.8.2), specifically DifferentialEquations.jl [33], stochastic differential equation solvers [34,35], and Prism (Version 8.0; GraphPad Software Inc., La Jolla, CA). For comparing NDS and raw c-Fos levels, a one-way analysis of variance (ANOVA) with a post-hoc Tukey test was used to determine significance of data. Statistical significance was met at $p<0.05$.

Non-Negative Matrix Factorization

For each of the N rats and the resulting c-Fos positivity in each of the M brain regions, we can construct a matrix $\mathbf{C} \in \mathbb{R}_{\geq 0}^{N \times M}$ with only positive real entries. Since some brain regions were not able to be properly visualized in some rats, we used k-nearest neighbors imputation to fill in the missing values. We assume the c-Fos levels in a given brain region are independently and identically distributed across rats. Naturally, the matrix can be thought of as encoding "time" since CA along rows (since each rat is sacrificed at a specific time) and the neural activity in a given region across columns. Using the `nnmf()` function in MATLAB, we can then re-express the matrix as

$$\mathbf{C} \approx \mathbf{W}\mathbf{H}$$

where $\mathbf{W} \in \mathbb{R}_{\geq 0}^{N \times k}$, $\mathbf{H} \in \mathbb{R}_{\geq 0}^{k \times M}$, and k is the rank of the approximation, or number of "modes" to decompose $\mathbf{C}$ into. We choose $k = 2$ as a trade-off between accuracy of reconstruction and interpretability of the latent modes.

Multivariate-Gaussian Approximation

Given the matrix $\mathbf{W}$, which holds for each rat a point in the 2-D plane that encodes a lower rank representation of the full c-Fos activity, we would like to model the distribution of points in the plane at a given post-CA time. The post-CA time for each rat is encoded as a vector $\mathbf{t} \in \mathbb{R}^N$. Therefore, we can write

$$p(\mathbf{w}_i | t_i) \sim \mathrm{N}(\boldsymbol{\mu}_i, \boldsymbol{\Sigma}_i)$$

as the distribution of the latent c-Fos levels in the 2-D plane ($\mathbf{w}_i$, row i in $\mathbf{W}$) for a given post-CA time t_i, where $\boldsymbol{\mu}_i$ is the conditional mean and $\boldsymbol{\Sigma}_i$ the conditional covariance matrix of a multivariate normal distribution. We choose $\boldsymbol{\Sigma}_i$ to be diagonal due to low power to estimate correlations. We use the `robustcov()` function in MATLAB with the Orthogonalized Gnanadesikan-Kettenring (OGK) method to compute $\boldsymbol{\mu}_i$ and $\boldsymbol{\Sigma}_i$ in the face of outliers.

To sample in the full M-dimensional c-Fos space, we can project the multivariate Gaussian up using an affine projection:

$$p(\mathbf{c}_i | t_i) \sim \mathrm{N}(\boldsymbol{\mu}_i \mathbf{H}, \mathbf{H}^\top \boldsymbol{\Sigma}_i \mathbf{H}).$$

Note, the matrix $\boldsymbol{\chi}_i = \mathbf{H}^\top \boldsymbol{\Sigma}_i \mathbf{H}$ is now a robust estimate of the full covariance matrix between c-Fos levels in all M brain regions for each time t_i, and can be used to estimate functional connectivity. Finally, to project the samples back into the 2-D latent plane, we can write

$$\mathbf{w}_i \approx \mathbf{c}_i \mathbf{H}^+$$

where $\mathbf{H}^+$ is the Moore-Penrose pseudoinverse (since $\mathbf{H}$ is not square).

Stochastic Differential Equation Model

Although we have defined estimates of the distribution $p(\mathbf{w}_i | t_i)$ at discrete times, to maximize the predictive power of our model we could use some interpolation scheme to "fill-in" the dynamics and thus have a continuous time model. A stochastic differential equation (SDE) model was constructed in Julia to model the dynamics in the latent plane. The model equations were expressed as

$$\begin{aligned} dw_1 &= (-0.1 w_1 + a\delta_{0 \leq t < 0.5})\, dt + (0.008 w_1 + 2) dW \\ dw_2 &= (-0.1 w_2 + b w_1 + c\delta_{t \geq 24})\, dt + 0.1 w_2 dW \end{aligned}$$

where dW is a Wiener process, and δ_x is an indicator function that evaluates to 1 when the condition x is satisfied, and time is in hours since CA. Coefficients with fixed values were first fit by hand to get good initial agreement between the SDE distribution and data. Then, the remaining coefficients with variable values were passed into a Simulated Annealing optimizer for global optimization (using Optim.jl and Optimization.jl). The method of moments was used such that the loss,

$$\mathcal{L}(a,b,c) = \sum_i (\boldsymbol{\mu}_i - \mathbb{E}[\mathbf{w}(t_i)])^2 + (\boldsymbol{\Sigma}_{1,1,i} - \mathrm{Var}(w_1(t_i)))^2 + (\boldsymbol{\Sigma}_{2,2,i} - \mathrm{Var}(w_2(t_i)))^2$$

,

was minimized with respect to $p(\mathbf{w}_i|t_i)$ estimated from the data.

Acknowledgements

References

Bibliography

1. Karpenko A, Keegan J. Diagnosis of Coma. *Emerg Med Clin North Am*. 2021;39(1):155-172. doi:10.1016/j.emc.2020.09.009
2. Teasdale G, Jennett B. Assessment of coma and impaired consciousness. A practical scale. *Lancet*. 1974;2(7872):81-84. doi:10.1016/s0140-6736(74)91639-0
3. Virani SS, Alonso A, Benjamin EJ, et al. Heart Disease and Stroke Statistics-2020 Update: A Report From the American Heart Association. *Circulation*. 2020;141(9):e139-e596. doi:10.1161/CIR.0000000000000757
4. Committee on the Treatment of Cardiac Arrest: Current Status and Future Directions, Board on Health Sciences Policy, Institute of Medicine. *Strategies to Improve Cardiac Arrest Survival: A Time to Act*. (Graham R, McCoy MA, Schultz AM, eds.). National Academies Press (US); 2015. doi:10.17226/21723
5. Nielsen N, Wetterslev J, Cronberg T, et al. Targeted temperature management at 33°C versus 36°C after cardiac arrest. *N Engl J Med*. 2013;369(23):2197-2206. doi:10.1056/NEJMoa1310519
6. Marion DW. Coma due to cardiac arrest: prognosis and contemporary treatment. *F1000 Med Rep*. 2009;1. doi:10.3410/M1-89
7. Kang Y-J, Tian G, Bazrafkan A, et al. Recovery from Coma Post-Cardiac Arrest Is Dependent on the Orexin Pathway. *J Neurotrauma*. 2017;34(19):2823-2832. doi:10.1089/neu.2016.4852
8. Moruzzi G, Magoun HW. Brain stem reticular formation and activation of the EEG. *Electroencephalogr Clin Neurophysiol*. 1949;1(4):455-473. doi:10.1016/0013-4694(49)90219-9
9. von Cramon D. Consciousness and disturbances of consciousness. *J Neurol*. 1978;219(1):1-13. doi:10.1007/BF00313364
10. Lindsley DB, Schreiner LH, Knowles WB, Magoun HW. Behavioral and EEG changes following chronic brain stem lesions in the cat. *Electroencephalogr Clin Neurophysiol*. 1950;2(4):483-498.
11. Nauta WJH. Hypothalamic regulation of sleep in rats; an experimental study. *J Neurophysiol*. 1946;9:285-316. doi:10.1152/jn.1946.9.4.285
12. Saper CB, Scammell TE, Lu J. Hypothalamic regulation of sleep and circadian rhythms. *Nature*. 2005;437(7063):1257-1263. doi:10.1038/nature04284

13. Arguinchona JH, Tadi P. Neuroanatomy, reticular activating system. In: *StatPearls*. StatPearls Publishing; 2022.

14. Cabrera G, Cavelli M, Lopez C, et al. Wakefulness-promoting role of the inferior colliculus. *Behav Brain Res*. 2013;256:82-94. doi:10.1016/j.bbr.2013.07.049

15. Onodera H, Kogure K, Ono Y, Igarashi K, Kiyota Y, Nagaoka A. Proto-oncogene c-fos is transiently induced in the rat cerebral cortex after forebrain ischemia. *Neurosci Lett*. 1989;98(1):101-104. doi:10.1016/0304-3940(89)90381-9

16. Bullitt E. Expression of c-fos-like protein as a marker for neuronal activity following noxious stimulation in the rat. *J Comp Neurol*. 1990;296(4):517-530. doi:10.1002/cne.902960402

17. Herrera DG, Robertson HA. Activation of c-fos in the brain. *Prog Neurobiol*. 1996;50(2-3):83-107.

18. Kiessling M, Stumm G, Xie Y, et al. Differential transcription and translation of immediate early genes in the gerbil hippocampus after transient global ischemia. *J Cereb Blood Flow Metab*. 1993;13(6):914-924. doi:10.1038/jcbfm.1993.114

19. Munell F, Burke RE, Bandele A, Gubits RM. Localization of c-fos, c-jun, and hsp70 mRNA expression in brain after neonatal hypoxia-ischemia. *Brain Res Dev Brain Res*. 1994;77(1):111-121. doi:10.1016/0165-3806(94)90218-6

20. Cho S, Park EM, Kim Y, et al. Early c-Fos induction after cerebral ischemia: a possible neuroprotective role. *J Cereb Blood Flow Metab*. 2001;21(5):550-556. doi:10.1097/00004647-200105000-00009

21. Bokesch PM, Halpin DP, Ranger WR, et al. Immediate-early gene expression in ovine brain after hypothermic circulatory arrest: effects of aptiganel. *Ann Thorac Surg*. 1997;64(4):1082-1087; discussion 1088. doi:10.1016/s0003-4975(97)00801-1

22. Zhang H, Li L, Xu G-Y, et al. Changes of c-fos, malondialdehyde and lactate in brain tissue after global cerebral ischemia under different brain temperatures. *J Huazhong Univ Sci Technol Med Sci*. 2014;34(3):354-358. doi:10.1007/s11596-014-1282-4

23. Azadian M, Tian G, Bazrafkan A, et al. Overnight caloric restriction prior to cardiac arrest and resuscitation leads to improved survival and neurological outcome in a rodent model. *Front Neurosci*. 2020;14:609670. doi:10.3389/fnins.2020.609670

24. Lee DE, Lee LG, Siu D, et al. Neural Correlates of Consciousness at Near-Electrocerebral Silence in an Asphyxial Cardiac Arrest Model. *Brain Connect*. 2017;7(3):172-181. doi:10.1089/brain.2016.0471

25. Wilson RH, Crouzet C, Torabzadeh M, et al. High-speed spatial frequency domain imaging of rat cortex detects dynamic optical and physiological properties following cardiac arrest and resuscitation. *Neurophotonics*. 2017;4(4):045008. doi:10.1117/1.NPh.4.4.045008

26. Crouzet C, Wilson RH, Lee D, et al. Dissociation of cerebral blood flow and femoral artery blood pressure pulsatility after cardiac arrest and resuscitation in a rodent model: implications for neurological recovery. *J Am Heart Assoc*. 2020;9(1):e012691. doi:10.1161/JAHA.119.012691

27. Crouzet C, Wilson RH, Bazrafkan A, et al. Cerebral blood flow is decoupled from blood pressure

and linked to EEG bursting after resuscitation from cardiac arrest. *Biomed Opt Express*. 2016;7(11):4660-4673. doi:10.1364/BOE.7.004660

28. Medvedeva YV, Yin HZ, Bazrafkan A, et al. Blocking mitochondrial Zn2+ accumulation after ischemia reduces mitochondrial dysfunction and neuronal injury. *J Neurosci*. 2022;42(26):5281-5292. doi:10.1523/JNEUROSCI.0874-21.2022
29. Yin HZ, Wang H-L, Ji SG, et al. Rapid intramitochondrial zn2+ accumulation in CA1 hippocampal pyramidal neurons after transient global ischemia: A possible contributor to mitochondrial disruption and cell death. *J Neuropathol Exp Neurol*. 2019;78(7):655-664. doi:10.1093/jnen/nlz042
30. Han S, Contreras MI, Bazrafkan A, et al. Cortical Anoxic Spreading Depolarization During Cardiac Arrest is Associated with Remote Effects on Peripheral Blood Pressure and Postresuscitation Neurological Outcome. *Neurocrit Care*. 2022;37(Suppl 1):139-154. doi:10.1007/s12028-022-01530-2
31. Parvizi J, Damasio A. Consciousness and the brainstem. *Cognition*. 2001;79(1-2):135-160. doi:10.1016/S0010-0277(00)00127-X
32. Vanini G, Watson CJ, Lydic R, Baghdoyan HA. Gamma-aminobutyric acid-mediated neurotransmission in the pontine reticular formation modulates hypnosis, immobility, and breathing during isoflurane anesthesia. *Anesthesiology*. 2008;109(6):978-988. doi:10.1097/ALN.0b013e31818e3b1b
33. Rackauckas C, Nie Q. DifferentialEquations.jl – A Performant and Feature-Rich Ecosystem for Solving Differential Equations in Julia. *J Open Res Softw*. 2017;5. doi:10.5334/jors.151
34. Rackauckas C, Nie Q. Adaptive methods for stochastic differential equations via natural embeddings and rejection sampling with memory. *Discrete Continuous Dyn Syst Ser B*. 2017;22(7):2731-2761. doi:10.3934/dcdsb.2017133
35. Rackauckas C, Nie Q. Stability-Optimized High Order Methods and Stiffness Detection for Pathwise Stiff Stochastic Differential Equations. In: *2020 IEEE High Performance Extreme Computing Conference (HPEC)*. IEEE; 2020:1-8. doi:10.1109/HPEC43674.2020.9286178